ACS NANO

www.acsnano.org

ARTICLE

Ultrasensitive and Selective Field-Effect Transistor-Based Biosensor Created by Rings of MoS_2 Nanopores

Heekyeong Park,[¶] Seungho Baek,[¶] Anamika Sen, Bongjin Jung, Junoh Shim, Yun Chang Park, Luke P. Lee,* Young Jun Kim,* and Sunkook Kim*

Cite This: *ACS Nano* 2022, 16, 1826−1835

Read Online

ACCESS | Metrics & More | Article Recommendations | Supporting Information

ABSTRACT: The ubiquitous field-effect transistor (FET) is widely used in modern digital integrated circuits, computers, communications, sensors, and other applications. However, reliable biological FET (bio-FET) is not available in real life due to the rigorous requirement for highly sensitive and selective bio-FET fabrication, which remains a challenging task. Here, we report an ultrasensitive and selective bio-FET created by the nanorings of molybdenum disulfide (MoS_2) nanopores inspired by nuclear pore complexes. We characterize the nanoring of MoS_2 nanopores by scanning transmission electron microscopy, Raman, and X-ray photoelectron spectroscopy spectra. After fabricating MoS_2 nanopore rings-based bio-FET, we confirm edge-selective functionalization by the gold nanoparticle tethering test and the change of electrical signal of the bio-FET. Ultrahigh sensitivity of the MoS_2 nanopore edge rings-based bio-FET (limit of detection of 1 ag/mL) and high selectivity are accomplished by effective coupling of the aptamers on the nanorings of the MoS_2 nanopore edge for cortisol detection. We believe that MoS_2 nanopore edge rings-based bio-FET would provide platforms for everyday biosensors with ultrahigh sensitivity and selectivity.

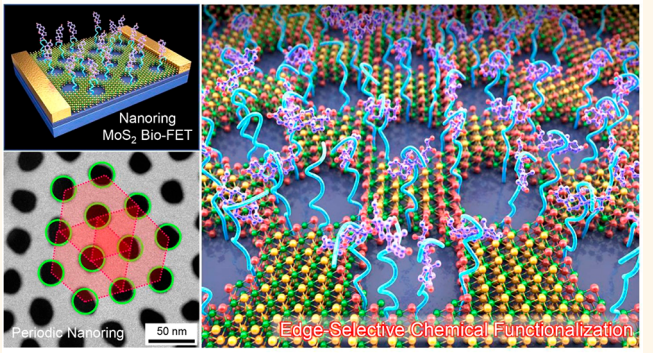

KEYWORDS: *MoS_2 bio-FET, nanopatterning, edge engineering, edge functionalization, ultrasensitive biosensor*

INTRODUCTION

The field-effect transistors (FETs) are extensively used as key elements of integrated circuits, computers, communications, and other applications. Especially, with high advantages of label-free, rapid, and ultrasensitive detection of target molecules,[1−3] FETs are highly desired as sensors, leading to a wide range of applications in medical care,[4] agriculture,[5] and environment.[6] With suitable modifications, biological FETs (bio-FETs) display extraordinarily sensitive interaction between target and receptor elements. In particular, the detection performance of bio-FETs is much affected by the structural and electrical characteristics of the channel materials, thereby indicating that assay performance can be further enhanced for example by introducing nanostructures in the channel.

With the advantages of retaining bandgaps compared to the most widely known two-dimensional (2D) nanomaterial, graphene with zero bandgap, transition metal dichalcogenides (TMDs) are considered promising materials for ultrasensitive biosensors.[7−9] In spite of the intrinsic carrier transport properties, however, the use of TMD materials for applications in biosensors has been limited due to the restraint in proper functional groups on their surface. The van der Waals force of the TMDs allows a physical adsorption of the receptor biomolecules on their surface.[10,11] However, these methods induce unstable and random binding of the receptors, resulting in loss of the target binding capacity and denaturation of the biomolecules. Therefore, mostly in TMD bio-FETs, grafting layers such as hafnium oxide (HfO_2),[7,12,13] aluminum oxide (Al_2O_3),[14,15] titanium oxide (TiO_2),[16] and electron-beam deposited gold nanoparticles layer[17] have been used to link receptor molecules on top of the TMD channels. However, the use of the interlayer increases the physical distance between the channel and the charged biomolecules and screens the

Received: September 19, 2021
Accepted: December 23, 2021
Published: December 29, 2021

Downloaded via TSINGHUA UNIV on November 13, 2022 at 10:41:46 (UTC).
See https://pubs.acs.org/sharingguidelines for options on how to legitimately share published articles.

ACS Publications

© 2021 American Chemical Society

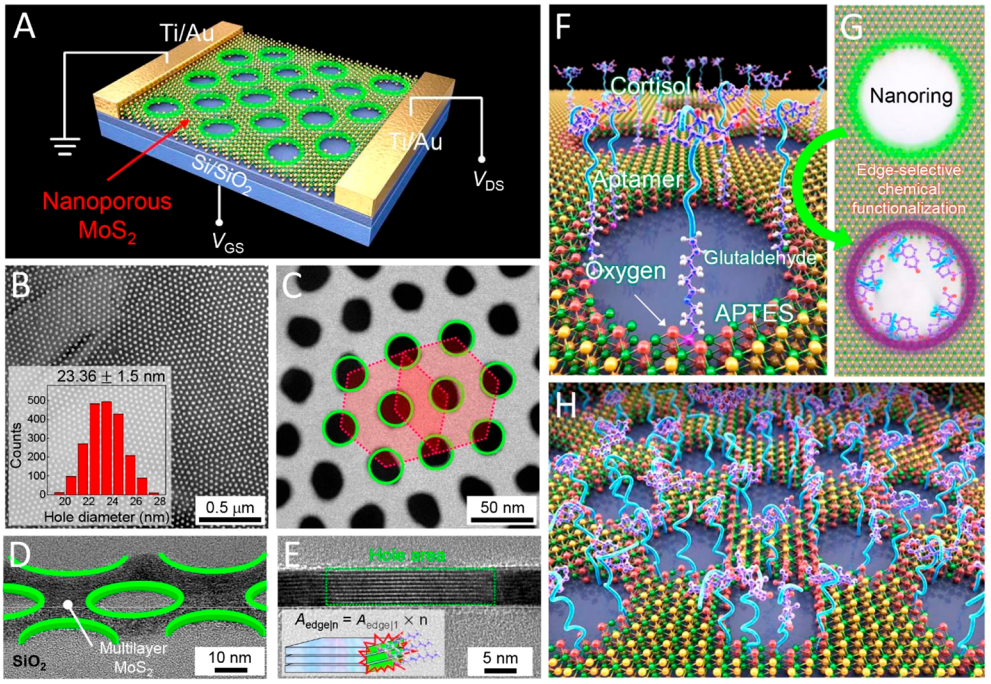

Figure 1. Ultrasensitive and selective bio-FET created by the nanoring edges of MoS_2 nanopores. (A) Schematic diagram of Bio-FET with the nanoring edges of MoS_2 nanopores. (B and C) STEM images of nanoporous MoS_2 films (inset of panel B, statistical distribution of nanopore diameters on the MoS_2). (D and E) Cross-sectional STEM images of MoS_2 nanopore edge with multiple layers (inset of panel E, an increment in edge area by using multilayer MoS_2). (F) Selective edge functionalization of aptamer-cortisol complexes on MoS_2 nanopore edges using APTES−glutaraldehyde chemistry. (G) Enhanced adsorption of aptamer-cortisol complexes on the nanoring of MoS_2 nanopore by selective functionalization. (H) Schematic diagram of multiple nanorings of MoS_2 nanopore edges with aptamer-cortisol complexes.

signaling charges caused by interaction between the receptor molecules and the target analytes,[18,19] which is manifested as reduced sensitivity. In addition, the interface defects between the channel and grafting layer produce incidental electric fields or parasitic coupling, further contributing to the lowering of sensitivity and reliability in bio-FETs.[20]

To circumvent the limitation in surface functionality of TMDs, several groups have proposed the bio-FETs using dispersed TMDs, in which the TMD nanoflakes or nanowires were overlapped to form the channel, to introduce abundant edges for the chemical surface modfification.[21,22] However, those devices are not suitable for biosensing electronics due to low stability, high noise level, and biotoxicity derived from the immoderate defects and impurities. Fathi-Hafshejani et al.[23] reported the surface chemical adsorption of the biomolecules using selenium vacancies in tungsten diselenide (WSe_2). However, due to the limited yield in the selenium vacancies, this method is not expected to achieve ultrasensitive biosensors. We presented various TMD bio-FETs with their biomolecule adsorption method and detection property in Table S1.

In this work, we significantly augmented the edge area by adopting nanoporous structure in molybdenum disulfide (MoS_2) inspired by the selective biomolecular interactions of the nuclear pore complex. We applied block copolymer (BCP) lithography to utilize the newly generated dangling groups on the nanoring edges of the nanopores for the selective functionalization of nanorings' surface areas. Periodically arranged nanopores on MoS_2 and corresponding chemical changes in MoS_2 were confirmed by scanning transmission electron microscopy (STEM), Raman, and X-ray photoelectron spectroscopy (XPS) analysis. In particular, the direct covalent linkage between MoS_2 and the biorecognition elements was expected to manifest a highly sensitive interaction of the bio-FET with target molecules. Indeed, superb detection performance has resulted in a limit of detection (LOD) reacting to 1 ag/mL toward cortisol, both in human serum and artificial saliva.

RESULT AND DISCUSSION

MoS_2 Nanoporous Bio-FET for Sensitive and Selective Detection of Cortisol. Various nanomaterials have been used for high-performance biosensors by designing sophisticated schemes, often entailing complicated procedures.[24,25] However, in a simple scheme of bio-FET, we accomplished an ultrahigh sensitive detection by introducing nanoring edges of MoS_2 nanopores (Figure 1A). Multilayered MoS_2, an extension of 2D materials, although endowed with intrinsic morphological advantages as a sensor, is unsuitable for applications as biosensors due to the absence of functional groups upon which capture molecules can be attached. In this study, the functionality problem was overcome by generating an innumerable number of nanosized holes of uniform diameter on MoS_2. We established a procedure for fabricating the nanoporous MoS_2 using the self-assembled nanostructure of BCP film as a template (Figure S1). The BCP template's scanning electron microscopy (SEM) image is shown in Figure S2A, indicating the characteristic ordering of nanoporous structure over a large area with a uniform hole diameter (20.7 ± 1.3 nm). The template was treated with oxygen (O_2) plasma reactive-ion etching (RIE) to control the hole size of the BCP template. Before MoS_2 was perforated by boron trichloride (BCl_3) plasma RIE, a protective layer located on the MoS_2 was etched away by sulfur hexafluoride (SF_6) plasma RIE. The

https://doi.org/10.1021/acsnano.1c08255
ACS Nano 2022, 16, 1826−1835

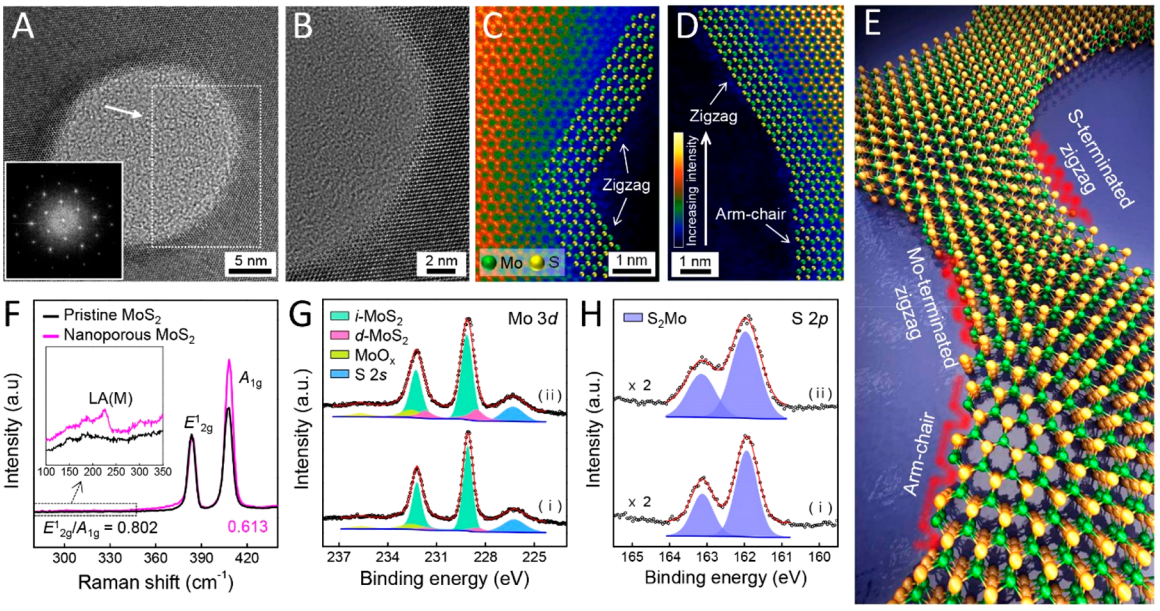

Figure 2. Structural and spectroscopic characterization of the nanoring edges of MoS_2 nanopores. (A) Plan-view STEM image of nanohole with (inset) FFT pattern corresponding to (100)-oriented hexagonal 2H MoS_2 plane. (B) High-magnification STEM image of the marked area in panel A. (C) High-magnification STEM image of zigzag edge of MoS_2 nanopores with intensity mapping profile. (D) Zigzag and arm-chair edges of MoS_2 nanopores with intensity mapping profile. (E) Schematic illustration of edge configurations of MoS_2 nanopores. (F) Raman spectra of pristine MoS_2 and nanoporous MoS_2. XPS spectra of (G) Mo 3d and (H) S 2p core level in multilayer MoS_2 (i) before and (ii) after nanopatterning.

detailed process is described in the Experimental Section and the SEM images of the MoS_2 surface for each process are shown in Figure S2B–D.

Figure 1B shows a low-magnification STEM image of the nanoporous MoS_2, in which nanopores were observed on the whole area of the multilayer MoS_2. The periodically organized nanopores have hexagonally packed ordering, as shown in Figure 1C. The structural uniformity of the nanopores was confirmed by measuring the diameter of 2200 nanopores from three different substrate samples, which was calculated to be 23.36 nm with a standard deviation of 1.5 nm (Inset of Figure 1B). Further, the vertically oriented nanopore structure across the multilayered MoS_2 was confirmed by a cross-sectional STEM image, as shown in Figure 1D,E. In Figure 1E, the nanopore edge areas look brighter than the unperforated areas due to differences in the distance from the surface MoS_2 atoms to the objective lens of the STEM. In the brighter nanopore area, 10 MoS_2 layers can be clearly observed. The edge area (A_{edge}) can be significantly increased by an increment of the layer numbers (n), facilitating an important enhancement in edge functionalization efficiency.

Figure 1F shows a conceptual illustration of the nanoring edge functionalization of cortisol aptamer and the detection of cortisol on the MoS_2 nanopores. The nanoring edges are oxidized by O_2 plasma treatment and functionalized with cortisol aptamer using the well-known (3-aminopropyl) triethoxysilane (APTES) - glutaraldehyde chemistry.[15] Thermodynamically unstable edges are easily functionalized with the chemical groups and a large number of aptamer-cortisol complexes are selectively captured on the nanoring edges of the MoS_2 nanopore (Figure 1G). The nanoring edges provide abundant binding sites for the cortisol aptamers, further leading to a significant increase in capturing of the cortisol molecules (Figure 1H). Those abundant biomolecular binding sites on the MoS_2 obtained by a myriad of nanoporous structures are thought to contribute to the concomitant augmentation of sensing performance in the nanoporous bio-FETs. In addition, in contrast to the previous MoS_2 bio-FETs where oxide layers were used for grafting probe molecules since no additional conjugating layer is used for the nanoporous MoS_2, the carrier modulation effect of the negative charge on cortisols seems to proceed in a highly efficient manner in the absence of the screening of the signal charge.

Spectroscopic Analysis of Nanoporous MoS_2. The atomic structure of MoS_2 nanoring was observed by STEM measurement. Figure 2A shows a highly magnified STEM image of the nanoring of the MoS_2 nanopore with a close-up view of the dashed area presented in Figure 2B. The fast Fourier transform (FFT) pattern extracted from Figure 2A suggests (100)-oriented hexagonal 2H MoS_2 film with AA′ stacking (inset of Figure 2A). To investigate the atomic configuration of the circular nanoring edges, an atomic-scale STEM observation of two sides of the circular nanoring was performed (Figures 2C,D). Indeed, the intensity mapping images exhibit anisotropically etched edge structures of the perforated MoS_2 multilayer. The atomic configurations of the top MoS_2 layer show both zigzag and armchair arrangements of Mo and S atoms at the nanoring edges. The atomic structures of each edge configuration are described in a schematic image of the nanopore in Figure 1E. Zigzag edges are classified into Mo-terminated and S-terminated zigzag according to the type of outermost atom. However, Mo-termination and S-termination are repeated layer by layer due to the AA′ stacking sequence of the MoS_2 films.

To study the effects of the newly formed morphological changes in MoS_2, a comparative analysis was performed for both the nanoporous and pristine MoS_2 films using Raman and XPS. In the Raman spectra (Figure 2F), two characteristic Raman peaks of the in-plane, E^1_{2g}, and out-of-plane, A_{1g}, vibrations were observed at 380 and 407 cm^{-1}, respectively, in

https://doi.org/10.1021/acsnano.1c08255
ACS Nano 2022, 16, 1826–1835

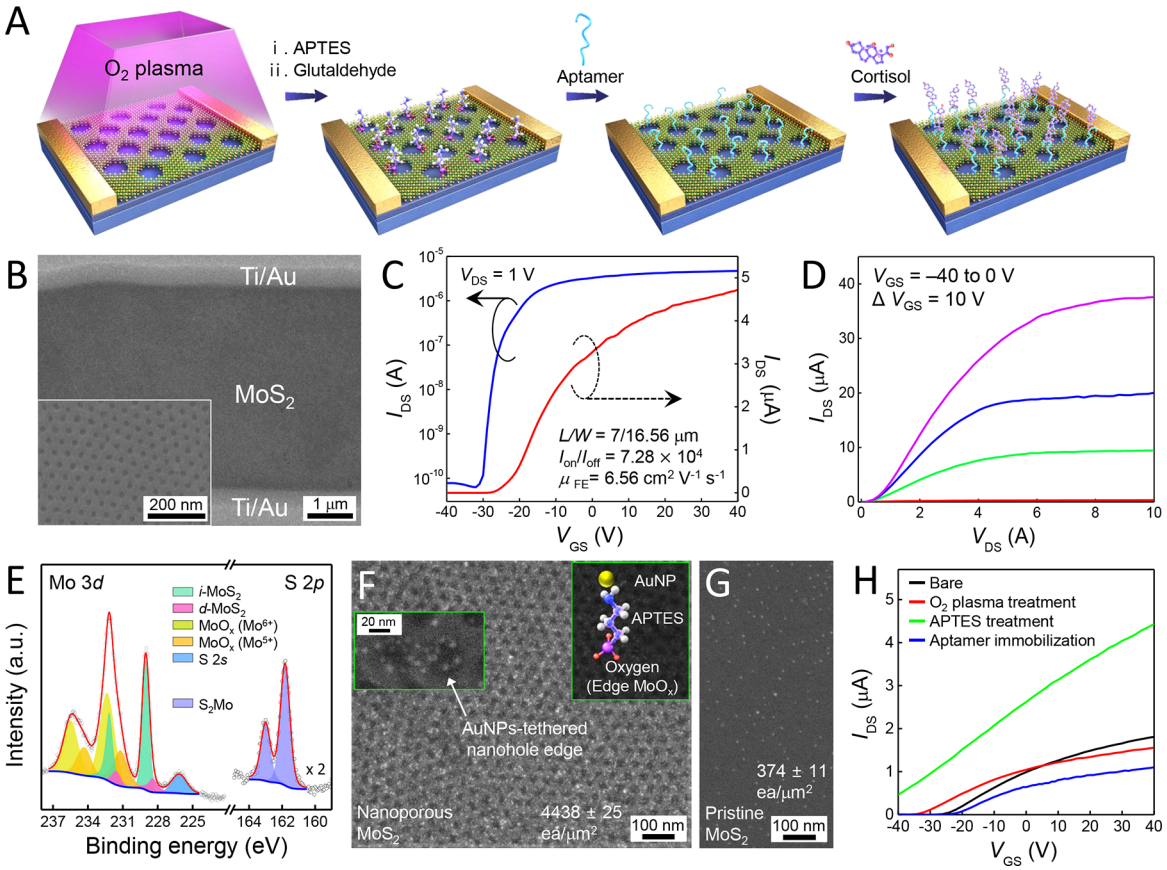

Figure 3. Preparation of MoS_2 bio-FET with nanopore edge for selective biomolecular detection. (A) Experimental process of functionalization of aptamer on the surface of nanoporous MoS_2 and detection of cortisol. (B) SEM images of nanoporous MoS_2 FET surface. (C) Transfer and (D) output characteristics of nanoporous MoS_2 FET. (E) XPS spectra of nanoporous MoS_2 after O_2 plasma RIE treatment. SEM images of (F) nanoporous MoS_2 and (G) pristine MoS_2 surface tethered with AuNPs of 5 nm on APTES-treated surface. (H) Transfer curves of the nanoporous MoS_2 bio-FET measured during functionalization processes.

both the pristine and the nanoporous MoS_2.[26] After perforation, the relative intensities of the in-plane and out-of-plane vibrations (E^1_{2g}/A_{1g}) decreased from 0.802 for the pristine to 0.613 for the nanoporous MoS_2. The lowering of E^1_{2g}/A_{1g} in the nanoporous MoS_2 well supports the presence of the newly generated nanopores and increase in the edge sites since A_{1g} vibration is preferentially excited to the E^1_{2g} vibration for edge-terminated films.[27,28] In addition, a new intense peak can be seen at ~227 cm^{-1} for the perforated MoS_2 (inset of Figure 2F). This band is a longitudinal acoustic (LA) branch at the M point of the Brillouin zone. It corresponds to disorder-induced Raman scattering in MoS_2, similar to the D band in defective graphene.[29,30] This band was activated on the nanoporous MoS_2 film because the edge defects were introduced into the MoS_2 lattice.

Figure 2G shows XPS analysis of the pristine (i) and the nanoporous (ii) MoS_2 films concerning their Mo 3d core levels. The corresponding S 2p spectra are shown in Figure 2H. In the Mo 3d spectra, the peak was deconvoluted into three different types of Mo ligands corresponding to the intrinsic MoS_2 (*i*-MoS_2), defective MoS_2 (*d*-MoS_2), and molybdenum oxide (MoO_x).[31,32] In the doublet of *i*-MoS_2, the maximum peak at around 229.10 eV (Mo^{4+} $3d_{5/2}$), which corresponds to 2H stoichiometric MoS_2 (ratio of S/Mo = 2), was observed in both the pristine and nanoporous MoS_2 films with high intensity. The maximum peak of the *d*-MoS_2 at 228.50 eV (Mo^{4+} $3d_{5/2}$) is relatively small, corresponding to the nonstoichiometric MoS_2 (S/Mo ratio <2) introduced by atomic defects on the film, such as vacancies and exposed edges.[31] These defect sites have electronic structures different from those of the intrinsic MoS_2 owing to the unstable energy state, resulting in peak excitation at lower binding energies. The atomic fraction of *d*-MoS_2 among the total Mo ligands was calculated to be 6.18% for the pristine MoS_2 film, which significantly increased to 15.82% for the nanoporous MoS_2 film (Table S2). This can be interpreted as the quantitative increase in the edge sites from the nanoporous MoS_2. In addition, the increase in nonstoichiometric MoS_2 in the nanoporous MoS_2 caused the characteristic broadening of the S 2p doublet, with a concomitant increase in the full width at half-maximum (fwhm) from 0.68 to 0.89. Contaminations on the active edge sites may occur during the etching process with BCl_3 plasma RIE. However, the absence of a Cl 2p peak in the nanoporous MoS_2 film (Figure S3) indicates that no contamination occurred during the BCl_3 etching process. In addition, the atomic fraction of Mo^{6+} 3d (MoO_x) at approximately 232.53 eV barely changed from 11.93% for the pristine to 11.49% for the nanoporous MoS_2, indicating that the active edge regions were not oxidized on exposure to the atmosphere.

Preparation of Nanoporous MoS_2 Bio-FET and Surface Functionalization for Cortisol Detection. Cortisol is a glucocorticoid steroid hormone secreted through the hypothalamus–pituitary–adrenal (HPA) axis. Repeated activation of the HPA axis has been reported to negatively affect

https://doi.org/10.1021/acsnano.1c08255
ACS Nano 2022, 16, 1826–1835

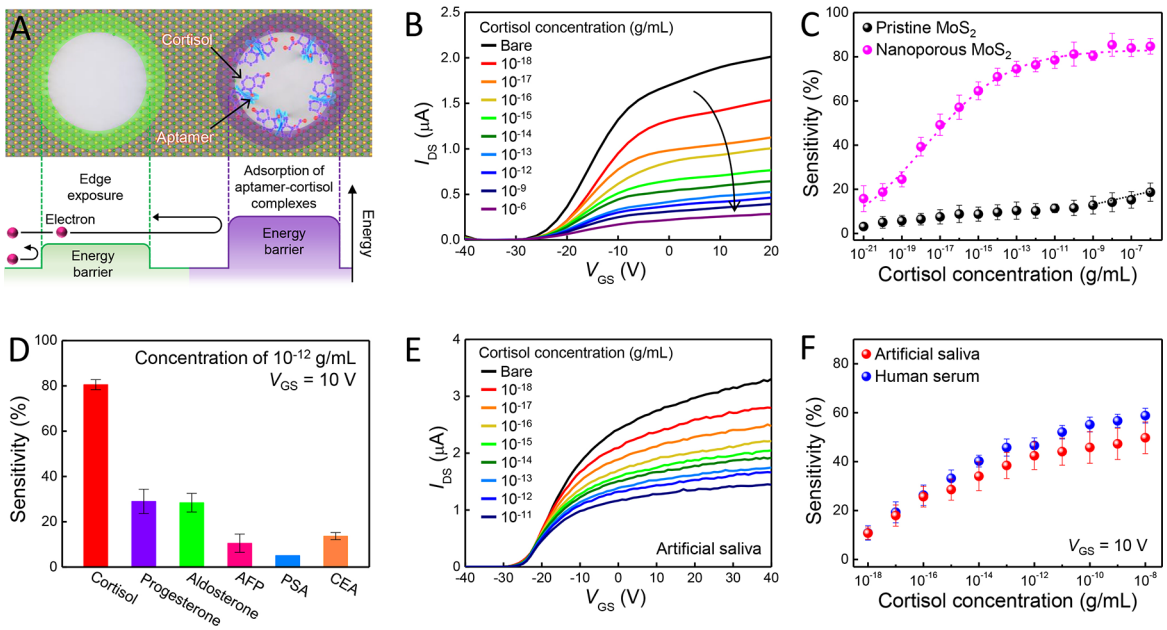

Figure 4. Application of MoS_2 nanopore edge-based bio-FETs for ultrasensitive and selective detection of cortisol. (A) Schematic images of MoS_2 nanopore and aptamer-cortisol adsorbed-nanopore, respectively, and related energy barrier height. (B) Transfer characteristics of the aptamer-immobilized on the nanoring edges of MoS_2 nanopore-based bio-FET with increasing cortisol concentrations. (C) A comparison of sensitivity of the pristine and the nanoporous MoS_2 bio-FETs according to cortisol concentrations. (D) Selectivity of the nanoporous MoS_2 bio-FETs for cortisol detection with several potentially interfering steroid hormones and antigens. (E) Detection characteristics of the nanoporous MoS_2 bio-FET for different concentrations of cortisol in artificial saliva. (F) Sensitivity of the bio-FETs in artificial saliva and real human serum.

mental health, causing major depressive disorder,[33] anxiety disorder,[34] and bipolar disorder.[35] The performance of the nanopatterned bio-FET was confirmed by studying its detection behavior toward cortisol. Figure 3A describes a general procedure for constructing the nanoporous MoS_2 bio-FET, in which a MoS_2 FET was treated with O_2 plasma and functionalized with cortisol aptamer using APTES- glutaraldehyde chemistry. Figure 3B is a SEM image of the MoS_2 FET presenting uniform nanopores across the channel area positioned between the two Ti/Au electrodes. Figure 3C depicts the transfer characteristics of the nanoporous MoS_2 FET in logarithmic (blue line), and linear (red line) scales measured under a gate voltage (V_{GS}) from −40 to 40 V at a drain voltage (V_{DS}) of 1 V. The length (L) and width (W) of the channel were 7 and 16.56 μm, respectively. It demonstrated an n-type semiconductor behavior with an on−off ratio (I_{on}/I_{off}) of 7.28×10^4 and field-effect mobility (μ_{FE}) of 6.56 $cm^2\ V^{-1}\ s^{-1}$. The output characteristics of the n-type nanoporous MoS_2 FET were shown in Figure 3D. We manufactured 20 different nanoporous MoS_2 FETs prepared from 20 different nanopatterned MoS_2. The statistical distribution of μ_{FE} for those MoS_2 FETs is depicted in Table S3, together with the values for I_{on}/I_{off}. The relatively low values of μ_{FE} in the nanoporous MoS_2 FET, compared to those (~100 $cm^2\ V^{-1}\ s^{-1}$) of the typical pristine multilayer MoS_2 FETs reported in the literature,[36] are thought to have been caused by an increase in carrier trapping and scattering in the MoS_2 channel due to increased defective edge areas of the nanopores.[37] However, stability of the bio-FETs turned out to be sound, as was confirmed by retaining the electrical performances even after repeated exposure to ambient air and phosphate-buffered saline (PBS) liquid (Figure S4A,B).

Treatment of O_2 plasma on the nanoporous MoS_2 FET was processed under mild conditions (5 sccm, 10 W, 15 s) since MoS_2 is prone to be damaged when exposed to O_2 plasma, which in turn may manifest into a detrimental effect on the electrical properties of the bio-FET. To understand the effect of the oxidation treatment, XPS analysis was carried out for both the nanoporous (Figure 3E) and the pristine (Figure S5) MoS_2. When O_2 plasma was treated for the nanoporous MoS_2, the atomic fraction of Mo^{4+} 3d was significantly reduced from 72.70% to 32.30% for i-MoS_2 and from 15.82% to 4.90% for d-MoS_2, respectively (Table S4). The atomic ratio of S^{2-} 2p to Mo^{4+} 3d also decreased from 2.04 to 1.87, signifying that the O_2 plasma treatment broke the bonding between Mo and S and replaces O at the location where S was (Table S4). With the generation of a new intense peak of MoO_x (Mo^{5+} 3d) at 231.33 eV, the total amount of MoO_x (Mo^{6+} 3d and Mo^{5+} 3d) increased from 11.49% to 62.80%. However, when the same treatment was done for pristine MoS_2, only a negligible amount of variation in the atomic ratio of S^{2-} 2p to Mo^{4+} 3d was observed from 2.06 to 2.01. From these, it can be conjectured that the oxidation in nanoporous MoS_2 occurs selectively at the newly generated edge regions in the nanoporous structure. However, the increase in MoO_x (Mo^{6+} 3d and Mo^{5+} 3d) peaks in the pristine corresponds to the relatively unstable oxide layer ($MoS_{2-y}O_y$)[38] on the MoS_2 basal plan. To find out if immobilization of the cortisol aptamer could be processed in the oxidized edge area of nanoporous MoS_2, possibly owing to the APTES chemistry, we investigated an assembly of 5 nm gold nanoparticles (AuNPs) on the APTES-functionalized nanoporous MoS_2 film (Figure 3F). For comparison, the same experiment was conducted on the pristine MoS_2 surface (Figure 3G). The density of AuNPs was measured to be 374 ± 11 ea/μm^2 for the pristine MoS_2 surface,

https://doi.org/10.1021/acsnano.1c08255
ACS Nano 2022, 16, 1826−1835

which was enhanced significantly to 4438 ± 25 ea/μm^2 for the nanoporous MoS_2 surface. In addition, it is noteworthy that the AuNPs were tethered favorably on the edge sites of nanopores rather than on the basal plane exposed between the nanopores (inset of Figure 3F), which indicates the efficient edge-selective functionalization using the APTES chemistry on the nanoporous MoS_2. Many papers have hypothesized the selective adsorption of analyte molecules at the edge based on the rich dangling bonds of the edge area.[39−41] However, we intuitively demonstrated the edge-selective functionalization through the AuNPs tethering experiment.

Figure 3H shows transfer curves of the nanoporous MoS_2 bio-FET measured during the functionalization process. The formation of MoO_x on edge induced the decrease in drain current (I_{DS}) at the on-state (V_{GS} > 0 V) due to *p*-type doping effect,[42,43] whereas the threshold voltage (V_{TH}) was negatively shifted due to an increase of the depletion mode as $MoS_{2-y}O_y$ was formed on the basal plane.[38] A significant increase in I_{DS} was also observed after the APTES treatment due to the *n*-type doping effect of APTES,[44] and this effect was negated when the cortisol aptamer was immobilized via glutaraldehyde treatment.

Sensing Performance of Nanoporous MoS_2 Bio-FET for Cortisol. Cortisol takes a negative charge under the measurement condition (pH 7.4) since the isoelectric point of cortisol is around 5.2.[45,46] The nanopore on the MoS_2 lattice provides energy barriers due to the conductivity difference between the MoS_2 basal plane and edge area (green hole and the corresponding energy diagram in Figure 4A).[37,47] The low conductivity of the edge regions is derived from scattering and trapping of mobile carriers at the newly generated trap states. We studied the generation of trap states in the nanoporous MoS_2 structure in a previous work.[48] When negatively charged cortisols are adsorbed at the nanoring edge area, the negative potential is accumulated on the MoS_2 edge area and induces depletion of the electron carriers by inhibiting the electron migration in the channel, further raising the energy band at the edge area.[49−51] Eventually, it seems to result in a higher energy barrier (purple hole and the corresponding energy diagram in Figure 4A). The sensing behavior of the nanoporous MoS_2 bio-FET was confirmed by gradually adding the precalculated amount of cortisol in a stepwise manner, so that the target concentration could be adjusted as required. Highly sensitive variations of transfer curves were observed in response to varying amounts of cortisol, as shown in Figure 4B. An increase in cortisol concentrations from 10^{-18} g/mL to 10^{-6} g/mL results in a gradual decrease of I_{DS} values due to increased energy barrier height.

To understand the effect of nanoring edges of MoS_2 nanopores on the sensing behavior, the sensing characteristics of the nanoporous and pristine MoS_2 FETs were compared (Figure 4C). The pristine MoS_2 bio-FETs were prepared by following the same surface treatment used for the nanoporous bio-FETs as described in Figure 3A. The sensing behavior of bio-FET with pristine MoS_2 is shown in Figure S6A, and current variations ($|I_{bare} - I_{cortisol}|$) of the pristine MoS_2 were compared with those of nanoporous MoS_2 bio-FET in Figure S6B, where I_{bare} and $I_{cortisol}$ are the I_{DS} values before and after the addition of cortisol, respectively, at a V_{GS} of 10 V. The sensitivity was calculated based on $(|I_{bare} - I_{cortisol}|)/I_{bare} \times 100$, at a V_{GS} of 10 V. A rather typical S-shaped response pattern was observed for the nanoporous MoS_2 FETs with a steep linear mode observed between 10^{-18} and 10^{-14} g/mL in cortisol concentration, while a slight hint of plateauing behavior was revealed at a low concentration range. In contrast, for the pristine MoS_2 FETs, no such apparent shape pattern was observed with only a slight hint of slope mode starting at around 10^{-9} g/mL of cortisol concentration. The two curves of the sensing behavior well support the surprisingly huge amount of enhancement effect in sensing performance of the MoS_2 nanoporous structure at least up to 10^9 times that of the pristine MoS_2.

The reliability of the nanoporous bio-FET was examined by studying the extent of nonspecific binding and selectivity using potentially interfering biomolecules. To understand the level of nonspecific interaction that might have been generated due to nanopore formation in MoS_2, cortisol detection was performed using nanoporous FETs in the absence of the aptamer capture molecules, specifically the nanoporous MoS_2 FET in which the surface chemistry was altered only up to the functionalization step of glutaraldehyde. No appreciable signal change was detected (Figure S7), suggesting that nonspecific interaction was negligible.

In addition, the selectivity of the nanoporous MoS_2 bio-FET for target cortisol was evaluated by measuring the electrical signals on exposure to potentially interfering biomolecules, including steroid hormones of progesterone and aldosterone, and protein biomarkers of alpha-fetoprotein (AFP), prostate specific antigen (PSA), and carcinoembryonic antigen (CEA) (Figure 4D). The sensitivity values after exposure to the protein antigens and the steroid hormones were noticeably lower than that of the cortisol. However, in the case of the steroid hormones, relatively increased sensitivity values were observed than for the proteins. It is worthwhile to note that the chemical structure of cortisol is very similar to that of progesterone and aldosterone.

One major advantage of using cortisol as a biomarker is the diverse availability of its biological fluids, including serum, urine, sweat, and saliva. In particular, measuring cortisol concentration in saliva has considerable merits, including being a patient-friendly noninvasive detection method and direct measurement of free unbound cortisol, which is a biologically active form; 90% of cortisol circulates in complexation with globulin.[52] To study the applicability of the nanoporous MoS_2 bio-FET in the clinical environment, the detection behavior of the bio-FET was examined in the media of artificial saliva and human serum. Figure 4E shows $I_{DS}-V_{GS}$ curves when the detection test was performed by varying the amount of cortisol from 10^{-18} g/mL to 10^{-8} g/mL in artificial saliva including the control test. Well-separated signals are evident, especially at a low concentration range with a gradual decrease in distance between signals at a higher concentration window. This tendency was somewhat more pronounced in artificial saliva than in human serum (Figure 4F). The $I_{DS}-V_{GS}$ curves for real human are shown in Figure S8. Compared with the results from the buffer test, the detection performance in the artificial saliva and serum seemed to have decreased to some extent, especially in the low concentration range, due to an inhibiting effect of innumerable types of biological entities and salt components contained in the saliva and serum. Those coexisting species adsorb onto a sensing interface nonspecifically and cause an adverse effect in the interaction of the probe molecules with the target molecules.[53,54] However, the LOD remained at 10^{-18} g/mL with linearity ranging up to 10^{-12} g/mL in those biological fluids. We solidified the excellent performance of the nanoring MoS_2 bio-FETs by comparing

https://doi.org/10.1021/acsnano.1c08255
ACS Nano 2022, 16, 1826−1835

with various types of cortisol sensors in terms of sensitivity and selectivity, as shown in Table S5. The nanoring MoS_2 bio-FETs offer significant advantages over other sensors with a wide detection range, ultralow LOD, and superb selectivity.

CONCLUSION

We accomplished an ultrasensitive and selective bio-FET by the nanorings of MoS_2 nanopores inspired by nuclear pore complexes. *Via* BCP nanotemplates, periodically organized nanopores were constructed on the MoS_2, thus providing abundant nanoring edges around the nanopores. While the generation of nanoring edge sites on the MoS_2 surface resulted in degradation of the electrical performance for FET, ultrahigh sensitivity was accomplished as a bio-FET due to enabling functionalization on the newly generated edges in the nanopatterned MoS_2. In addition, the nanoporous bio-FET functionalized with aptamer exhibited excellent selectivity for cortisol compared to other steroids and antigens, including progesterone, aldosterone, AFP, PSA, and CES. Clinical applicability was also confirmed by performing the test on artificial saliva and actual human serum. We confirmed the enhanced performance of the nanoporous MoS_2 bio-FET by realizing an ultrasensitive LOD of 1 ag/mL. With such a superb detection performance, the nanopatterned MoS_2 bio-FET may be applied for polymerase chain reaction-free detection of biomarkers.

EXPERIMENTAL METHODS

Fabrication of Nanoporous MoS_2 FET. The general fabrication process of the nanoporous MoS_2 consists of organizing the BCP nanopattern on MoS_2, etching the MoS_2, and subsequently removing the upper BCP layers. Multilayer MoS_2 nanosheets were placed on a Si/SiO_2 substrate by mechanical exfoliation from bulk MoS_2. A 10 nm thick SiO_2 layer was deposited onto the MoS_2 nanosheets using an electron-beam (e-beam) evaporator. A 1 wt % solution of poly(styrene-*r*-methyl methacrylate) (PS-*r*-PMMA) (M_n = 8500 M_w/M_n = 1.45, styrene content of 66%, α-hydroxyl-ω-TEMPO moiety terminated) random copolymer (RCP) in toluene was spin-coated on the MoS_2 films at 3000 rpm, followed by substrate annealing at 250 °C for 2 h under vacuum and finally rinsing with toluene. RCP was used as a grafting layer to produce neutral and uniform wetting of the BCP film on the substrate. A solution of 1 wt % poly(styrene-*b*-methyl methacrylate) (PS-*b*-PMMA) (PS/PMMA = 55 000:22 000, M_w/M_n = 1.09) BCP in toluene was also spin-coated with the same protocol as RCP and annealed at 230 °C. The PMMA portions in the BCP thin film were decomposed by UV irradiation (wavelength of 254 nm) for 30 min and finally dissolved in acetic acid solution. O_2 plasma RIE (10 sccm, 10 W, 10 s) was applied to the surface of BCP. SF_6 plasma RIE (10 sccm, 200 W, 15 s) was carried out to punch nanopores on the SiO_2 layer. Subsequently, BCl_3 plasma RIE (10 sccm, 100 W) was used to make MoS_2 nanopores, with the plasma treatment time-varying with the thickness of MoS_2. At the end of the process, the substrate was submerged in BOE for 1 s to eliminate the remaining SiO_2 and BCP on the MoS_2. To construct the FET on the prepared nanoporous MoS_2, the source and drain were prepatterned by photolithography and a lift-off process, followed by deposition of Ti (20 nm)/Au (100 nm) by e-beam evaporation. Pristine MoS_2 bio-FET was fabricated by the deposition of the Ti/Au electrode on exfoliated MoS_2.

Characterizations. Microstructural studies of the nanoporous MoS_2 were conducted using STEM (HD-2300A, Hitachi) with an accelerating voltage of 200 kV. For plane-view observation, the nanoporous MoS_2 films were transferred onto Cu grids coated with a lacey carbon film. A cross-sectional view was observed by milling the sample using a single-beam focused ion-beam (FB-2100, Hitachi). Low-magnification surface images were obtained by SEM operated at an acceleration voltage of 15 kV and working distance of 8 mm. Raman spectroscopy (ALPHA300, WITec) was used to identify the formation of edge sites on MoS_2 nanosheets. A laser beam with a spot diameter of 1 μm and excitation wavelength of 532 nm was used, and the instrument spectral resolution was approximately 1 cm^{-1}. The chemical states of the MoS_2 films were explored by XPS (K-Alpha, Thermo Fisher Scientific) using an Al Kα source. All electrical measurements were carried out using a semiconductor characterization analyzer (4200-SCS, Keithley) equipped with a probe station for sample loading and electrode contact.

MoS_2 Surface Modification and Biosensing Process. Specific detection of cortisol was facilitated by functionalizing an aptamer, which is a bioreceptor for cortisol, on the channel surface of the nanoporous MoS_2 bio-FET. The aptamer (Bioneer) was dissolved in Tris-HCl (pH 8.0) solution to obtain a concentration of 10^{-6} g/mL. The MoS_2 bio-FET was first exposed to O_2 plasma (10 sccm, 10 W, 15 s) for edge oxidation. The MoS_2 was then functionalized with APTES by treating with a solution of 0.4 mL of APTES in a 19:1 (v/v) mixture of ethanol and deionized (DI) water for 3 h. Subsequently, the device was rinsed in ethanol and dried at 120 °C for 15 min. To convert the amine functional group of APTES to an aldehyde group, the device was immersed in 4.5 mL of glutaraldehyde solution consisting of 0.1 g of $NaCNBH_4$, 1 tablet of PBS, and 200 mL of DI water, for 2 h, followed by rinsing in DI water. The device was incubated overnight in a 10^{-6} g/mL aptamer solution at 4 °C. To prevent nonspecific binding, 1% (w/v) casein blocker (Thermo Fisher Scientific) was added to the device for 1 h at room temperature. For the detection of cortisol, 16 different concentrations of cortisol solution (Sigma-Aldrich) ranging from 10^{-21} g/mL to 10^{-6} g/mL were dissolved in PBS solution (pH 7.4). Each cortisol solution was dropped onto the device for 30 min and subsequently rinsed and dried for electrical measurements.

Detection in Saliva and Human Serum. To understand the sensing behavior in the biological environment of saliva and serum, different concentrations of cortisol were dissolved in artificial saliva and real human serum. Real human serum was purchased from Sigma-Aldrich. Artificial saliva was prepared by dissolving cellulose, 5 mM NaCl, 1 mM $CaCl_2$, 15 mM KCl, 1 mM citric acid, 1.1 mM KSCN, and 4 mM NH_4Cl in distilled water.

ASSOCIATED CONTENT

Supporting Information

The Supporting Information is available free of charge at https://pubs.acs.org/doi/10.1021/acsnano.1c08255.

Comparison of the nanoporous MoS_2 bio-FET with other 2D TMDs bio-FETs; fabrication method and SEM images of MoS_2 surfaces for each fabrications processes; additional XPS analysis data of the nanoporous MoS_2 films; statistical distribution of electrical characteristics of the nanoporous MoS_2 bio-FETs and device stability tests in air and liquid environments; comparison of XPS spectra between the pristine and nanoporous MoS_2 films before and after O_2 plasma treatment; additional supporting information on the biomolecular sensing performances of the nanoporous MoS_2 bio-FETs; comparison of sensing performances of several cortisol biosensors with the nanoporous MoS_2 biosensor (PDF)

AUTHOR INFORMATION

Corresponding Authors

Luke P. Lee − *Harvard Institute of Medicine, Harvard Medical School, Harvard University, Brigham and Women's Hospital, Boston, Massachusetts 02115, United States; Department of Biophysics, Institute of Quantum Biophysics, Sungkyunkwan University (SKKU), Suwon 16419, Republic of Korea; Department of Bioengineering, Department of*

https://doi.org/10.1021/acsnano.1c08255
ACS Nano 2022, 16, 1826−1835

Electrical Engineering and Computer Science, University of California at Berkeley, Berkeley, California 94720, United States; orcid.org/0000-0002-1436-4054; Email: lplee@bwh.harvard.edu

Young Jun Kim − *BioNano Health Guard Research Center, Daejeon 34141, Republic of Korea*; Email: junkim@kribb.re.kr

Sunkook Kim − *Department of Advanced Materials Science and Engineering, Sungkyunkwan University (SKKU), Suwon 16419, Republic of Korea;* orcid.org/0000-0003-1747-4539; Email: seonkuk@skku.edu

Authors

Heekyeong Park − *Harvard Institute of Medicine, Harvard Medical School, Harvard University, Brigham and Women's Hospital, Boston, Massachusetts 02115, United States; Department of Advanced Materials Science and Engineering, Sungkyunkwan University (SKKU), Suwon 16419, Republic of Korea;* orcid.org/0000-0002-7509-5740

Seungho Baek − *Department of Advanced Materials Science and Engineering, Sungkyunkwan University (SKKU), Suwon 16419, Republic of Korea*

Anamika Sen − *Department of Advanced Materials Science and Engineering, Sungkyunkwan University (SKKU), Suwon 16419, Republic of Korea*

Bongjin Jung − *Electronics and Telecommunications Research Institute (ETRI), Daejeon 34129, Republic of Korea*

Junoh Shim − *Department of Advanced Materials Science and Engineering, Sungkyunkwan University (SKKU), Suwon 16419, Republic of Korea*

Yun Chang Park − *Measurement and Analysis Division, National Nanofab Center (NNFC), Daejeon 16229, Republic of Korea*

Complete contact information is available at: https://pubs.acs.org/10.1021/acsnano.1c08255

Author Contributions

[¶]H.P. and S.B. contributed equally. L.P.L., Y.J.K., and S.K. conceived the project. H.P., and S.B. fabricated the nano-patterned MoS_2 bio-FETs and measured the electrical properties and sensing properties of the devices. A.S., and J.S. supported the experiments. B.J. provided the bimolecular resources. Y.C.P. contributed to structural characterizations of the MoS_2 films using STEM analysis.

Notes

The authors declare no competing financial interest.

Pre-print statement: This work has been preprinted as follows: Heekyeong Park; Seungho Baek; Bongjin Jeong; Anamika Sen; Sehwan Kim; Yun Chang Park; Sunkook Kim; Young Jun Kim. Nanomesh-Patterning on Multilayer MoS_2 Field-Effect Transistors for Ultra-Sensitive Detection of Cortisol. 2020, PREPRINT (ver. 1). Research Square. 10.21203/rs.3.rs-64919/v1 (02 September, 2020).

ACKNOWLEDGMENTS

This research was supported in part by the National Research Foundation of Korea (2021R1A2B5B02002167). This research was supported by a grant of the Korea Health Technology R&D Project through the Korea Health Industry Development Institute (KHIDI), funded by the Ministry of Health & Welfare, Republic of Korea (Grant No. HI19C1348).

REFERENCES

(1) Vigneshvar, S.; Sudhakumari, C. C.; Senthilkumaran, B.; Prakash, H. Recent Advances in Biosensor Technology for Potential Applications - An Overview. *Front. Bioeng. Biotechnol.* **1997**, *4*, 11.

(2) Perumal, V.; Hashim, U. Advances in Biosensors: Principle, Architecture and Applications. *J. Appl. Biomed.* **2014**, *12*, 1−15.

(3) Sarkar, D.; Banerjee, K. Proposal for Tunnel-Field-Effect-Transistor as Ultra-Sensitive and Label-Free Biosensors. *Appl. Phys. Lett.* **2012**, *100*, 143108.

(4) Poghossian, A.; Cherstvy, A.; Ingebrandt, S.; Offenhausser, A.; Schoning, M. J. Possibilities and Limitations of Label-Free Detection of DNA Hybridization with Field-Effect-Based Devices. *Sens. Actuators B Chem.* **2005**, *111*, 470−480.

(5) Rai, V.; Acharya, S.; Dey, N. Implications of Nanobiosensors in Agriculture. *J. Biomater. Nanobiotech.* **2012**, *3*, 315−324.

(6) Rodriguez-Mozaz, S.; Alda, M. J. L.; de Marco, M. − P.; Barcelo, D. Biosensors for Environmental Monitoring - A Global Perspective. *Talanta* **2005**, *65*, 291−297.

(7) Sarkar, D.; Liu, W.; Xie, X.; Anselmo, A. C.; Mitragotri, S.; Banerjee, K. MoS_2 Field-Effect Transistor for Next-Generation Label-Free Biosensors. *ACS Nano* **2014**, *8*, 3992−4003.

(8) Kalantar-zadeh, K.; Ou, J. Z.; Daeneke, T.; Strano, M. S.; Pumera, M.; Gras, S. L. Two-Dimensional Transition Metal Dichalcogenides in. *Biosystems. Adv. Funct.Mater.* **2015**, *25*, 5086−5099.

(9) Park, H.; Lee, H.; Jeong, S. H.; Lee, E.; Lee, W.; Liu, N.; Yoon, D. S.; Kim, S.; Lee, S. W. MoS_2 Field-Effect Transistor-Amyloid-$Beta_{(1-42)}$ Hybrid Device for Signal Amplified Detection of MMP-9. *Anal. Chem.* **2019**, *91*, 8252−8258.

(10) Lee, J.; Dak, P.; Lee, Y.; Park, H.; Choi, W.; Alam, M. A.; Kim, S. Two-Dimensional Layered MoS_2 Biosensors Enable Highly Sensitive Detection of Biomolecules. *Sci. Rep.* **2015**, *4*, 1−7.

(11) Lee, D.-W.; Lee, J.; Sohn, I. Y.; Kim, B.-Y.; Son, Y. M.; Bark, H.; Jung, J.; Choi, M.; Kim, T. H.; Lee, C.; Lee, N.-E. Field-Effect Transistor with a Chemically Synthesized MoS_2 Sensing Channel for Label-Free and Highly Sensitive Electrical Detection of DNA Hybridization. *Nano Res.* **2015**, *8*, 2340−2350.

(12) Nam, H.; Oh, B. − R.; Chen, P.; Chen, M.; Wi, S.; Wan, W.; Kurabayashi, K.; Liang, X. Multiple MoS_2 Transistors for Sensing Molecule Interaction Kinetics. *Sci. Rep.* **2015**, *5*, 10546.

(13) Wang, L.; Wang, Y.; Wong, J. I.; Palacios, T.; Kong, J.; Yang, H. Y. Functionalized MoS_2 Nanosheet-Based Field-Effect Biosensor for Label-Free Sensitive Detection of Cancer Marker Proteins in Solution. *Small* **2014**, *10*, 1101−1105.

(14) Zhang, Y.; Feng, D.; Xu, Y.; Yin, Z.; Dou, W.; Habiba, U. E; Pan, C.; Zhang, Z.; Mou, H.; Deng, H.; Mi, X.; Dai, N. DNA-Based Functionalization of Two-Dimensional MoS_2 FET Biosensor for Ultrasensitive Detection of PSA. *Appl. Surf. Sci.* **2021**, *548*, 149169.

(15) Park, H.; Han, G.; Lee, S. W.; Lee, H.; Jeong, S. H.; Naqi, M.; AlMutairi, A.; Kim, Y. J.; Lee, J.; Kim, W. − J.; Kim, S.; Yoon, Y.; Yoo, G. Label-Free and Recalibrated Multilayer MoS_2 Biosensor for Point-of-Care Diagnostics. *ACS Appl. Mater. Interfaces* **2017**, *9*, 43490−43497.

(16) Moudgil, A.; Singh, S.; Mishra, N.; Mishra, P.; Das, S. MoS_2/TiO_2 Hybrid Nanostructure-Based Field-Effect Transistor for Highly Sensitive, Selective, and Rapid Detection of Gram-Positive Bacteria. *Adv. Mater. Technol.* **2020**, *5*, 1900615.

(17) Liu, J.; Chen, X.; Wang, Q.; Xiao, M.; Zhong, D.; Sun, W.; Zhang, G.; Zhang, Z. Ultrasensitive Monolayer MoS_2 Field-Effect Transistor Based DNA Sensors for Screening of Down Syndrome. *Nano Lett.* **2019**, *19*, 1437−1444.

(18) Ahn, J. − H.; Choi, S. − J.; Im, M.; Kim, S.; Kim, C. − H.; Kim, J. − Y.; Park, T. J.; Lee, S. Y.; Choi, Y. − K. Charge and Dielectric Effects of Biomolecules on Electrical Characteristics of Nanowire FET Biosensors. *Appl. Phys. Lett.* **2017**, *111*, 113701.

(19) Liu, Y.; Dutton, R. W. Effects of Charge Screening and Surface Properties on Signal Transduction in Field Effect Nanowire Biosensors. *J. Appl. Phys.* **2009**, *106*, 014701.

(20) Kovacevic, G.; Pivac, B. Structure, Defects, and Strain in Silicon-Silicon Oxide Interfaces. *J. Appl. Phys.* **2014**, *115*, 043531.
(21) Mei, J.; Li, Y. − T.; Zhang, H.; Xiao, M. − M.; Ning, Y.; Zhang, Z. − Y.; Zhang, G. − J. Molybdenum Disulfide Field-Effect Transistor Biosensor for Ultrasensitive Detection of DNA by Employing Morpholino as Probe. *Biosens. Bioelectron.* **2018**, *110*, 71−77.
(22) Shariati, M.; Vaezjalali, M.; Sadeghi, M. Ultrasensitive and Easily Reproducible Biosensor Based on Novel Doped MoS_2 Nanowires Field-Effect Transistor in Label-Free Approach for Detection of Hepatitis B Virus in Blood Serum. *Anal. Chim. Acta* **2021**, *1156*, 338360.
(23) Fathi-Hafshejani, P.; Azam, N.; Wang, L.; Kuroda, M. A.; Hamilton, M. C.; Hasim, S.; Mahjouri-Samani, M. Two-Dimensional-Material-Based Field-Effect Transistor Biosensor for Detecting COVID-19 Virus (SARS-CoV-2). *ACS Nano* **2021**, *15*, 11461−11469.
(24) Song, Y.; Luo, Y.; Zhu, C.; Li, H.; Du, D.; Lin, Y. Recent Advances in Electrochemical Biosensors Based on Graphene Two-Dimensional Nanomaterials. *Biosens. Bioelectron.* **2016**, *76*, 195−212.
(25) Lan, L.; Yao, Y.; Ping, J.; Ying, Y. Recent Advances in Nanomaterial-Based Biosensors for Antibiotics Detection. *Biosens. Bioelectron.* **2017**, *91*, 504−514.
(26) Li, H.; Zhang, Q.; Yap, C. C. R.; Tay, B. K.; Edwin, T. H. T.; Olivier, A.; Baillargeat, D. From Bulk to Monolayer MoS_2: Evolution of Raman Scattering. *Adv. Funct. Mater.* **2012**, *22*, 1385−1390.
(27) Yun, T.; Jin, H. M.; Kim, D. − H.; Han, K. H.; Yang, G. G.; Lee, G. Y.; Lee, G. S.; Choi, J. Y.; Kim, I. − D.; Kim, S. O. 2D Metal Chalcogenide Nanopatterns by Block Copolymer Lithography. *Adv. Funct. Mater.* **2018**, *28*, 1804508.
(28) Kim, T.; Kim, D.; Choi, C. H.; Joung, D.; Park, J.; Shin, J. C.; Kang, S. − W. Structural Defects in a Nanomesh of Bulk MoS_2 Using an Anodic Aluminum Oxide Template for Photoluminescence Efficiency Enhancement. *Sci. Rep.* **2018**, *8*, 6648.
(29) Mignuzzi, S.; Pollard, A. J.; Bonini, N.; Brennan, B.; Gilmore, I. S.; Pimenta, M. A.; Richards, D.; Roy, D. Effect of Disorder on Raman Scattering of Single-Layer MoS_2. *Phys. Rev. B* **2015**, *91*, 195411.
(30) Frey, G. L.; Tenne, R.; Matthews, M. J.; Dresselhaus, M. S.; Dresselhaus, G. Raman and Resonance Raman Investigation of MoS_2 Nanoparticles. *Phys. Rev. B* **1999**, *60*, 2883.
(31) Kondekar, N. P.; Boebinger, M. G.; Woods, E. V.; McDowell, M. T. *In Situ* XPS Investigation of Transformations at Crystallographically Oriented MoS_2 Interfaces. *ACS Appl. Mater. Interfaces* **2017**, *9*, 32394−32404.
(32) Lin, H.; Yang, L.; Jiang, X.; Li, G.; Zhang, T.; Yao, Q.; Zheng, G. W.; Lee, J. Y. Electrocatalysis of Polysulfide Conversion by Sulfur-Deficient MoS_2 Nanoflakes for Lithium-Sulfur Batteries. *Energy Environ. Sci.* **2017**, *10*, 1476−1486.
(33) Kendler, K. S.; Karkowski, L. M.; Prescott, C. A. Causal Relationship between Stressful Life Events and the Onset of Major Depression. *Am. J. Psychiatry* **1999**, *156*, 837−841.
(34) Moreno-Peral, P.; Conejo-Ceron, S.; Motrico, E.; Rodriguez-Morejon, A.; Fernandez, A.; Garcia-Campayo, J.; Roca, M.; Serrano-Blanco, A.; Rubio-Valera, M.; Bellon, J. A. Risk Factors for the Onset of Panic and Generalised Anxiety Disorders in the General Adult Population: A Systematic Review of Cohort Studies. *J. Affect. Disord.* **2014**, *168*, 337−348.
(35) Agnew-Blais, J.; Danese, A. Childhood Maltreatment and Unfavourable Clinical Outcomes in Bipolar Disorder: A Systematic Review and Meta-Analysis. *Lancet Psychiat.* **2016**, *3*, 342−349.
(36) Kim, S.; Konar, A.; Hwang, W. − S.; Lee, J. H.; Lee, J.; Yang, J.; Jung, C.; Kim, H.; Yoo, J. − B.; Choi, J. − Y.; Jin, Y. W.; Lee, S. Y.; Jena, D.; Choi, W.; Kim, K. High-Mobility and Low-Power Thin-Film Transistors Based on Multilayer MoS_2 Crystals. *Nat. Commun.* **2012**, *3*, 1011.
(37) Chen, S.; Kim, S.; Chen, W.; Yuan, J.; Bashir, R.; Lou, J.; van der Zande, A. M.; King, W. P. Monolayer MoS_2 Nanoribbon Transistors Fabricated by Scanning Probe Lithography. *Nano Lett.* **2019**, *19*, 2092−2098.
(38) Jadwiszczak, J.; O'Callaghan, C.; Zhou, Y.; Fox, D. S.; Weitz, E.; Keane, D.; Cullen, C. P.; O'Reilly, L.; Downing, C.; Shmeliov, A.; Maguire, P.; Gough, J. J.; McGuinness, C.; Ferreira, M. S.; Bradley, A. L.; Boland, J. J.; Duesberg, G. S.; Nicolosi, V.; Zhang, H. Oxide-Mediated Recovery of Field-Effect Mobility in Plasma-Treated MoS_2. *Sci. Adv.* **2018**, *4*, eaao5031.
(39) Asai, M.; Ohba, T.; Iwanaga, T.; Kanoh, H.; Endo, M.; Campos-Delgado, J.; Terrones, M.; Nakai, K.; Kaneko, K. Marked Adsorption Irreversibility of Graphitic Nanoribbons for CO_2 and H_2O. *J. Am. Chem. Soc.* **2011**, *133*, 14880−14883.
(40) Keerthi, A.; Radha, B.; Rizzo, D.; Lu, H.; Diez Cabanes, V.; Hou, I. C. − Y.; Beljonne, D.; Cornil, J.; Casiraghi, C.; Baumgarten, M.; Müllen, K.; Narita, A. Edge Functionalization of Structurally Defined Graphene Nanoribbons for Modulating the Self-Assembled Structures. *J. Am. Chem. Soc.* **2017**, *139*, 16454−16457.
(41) Cho, K. M.; Cho, S. − Y.; Chong, S.; Koh, H. − J.; Kim, D. W.; Kim, J.; Jung, H. − T. Edge-Functionalized Graphene Nanoribbon Chemical Sensor: Comparison with Carbon Nanotube and Graphene. *ACS appl. Mater. Interfaces* **2018**, *10*, 42905−42914.
(42) Choudhary, N.; Islam, M. R.; Kang, N.; Tetard, L.; Jung, Y.; Khondaker, S. I. Two-Dimensional Lateral Heterohunction through Bandgap Engineering of MoS_2 *via* Oxygen Plasma. *J. Phys.: Condens. Matter* **2016**, *28*, 364002.
(43) Neal, A. T.; Pachter, R.; Mou, D. *P*-Type Conduction in Two-Dimensional MoS_2 *via* Oxygen Incorporation. *Appl. Phys. Lett.* **2017**, *110*, 193103.
(44) Kang, D. − H.; Kim, M. − S.; Shim, J.; Jeon, J.; Park, H. − Y.; Jung, W. − S.; Yu, H. − Y.; Pang, C. − H.; Lee, S.; Park, J. − H. High-Performance Transition Metal Dichalcogenide Photodetectors Enhanced by Self-Assembled Monolayer Doping. *Adv. Funct. Mater.* **2015**, *25*, 4219−4227.
(45) Ku, M.; Kim, J.; Won, J. − E.; Kang, W.; Park, Y. − G.; Park, J.; Lee, J. − H.; Cheon, J.; Lee, H. H.; Park, J. − U. Smart, Soft Contact Lens for Wireless Immunosensing of Cortisol. *Sci. Adv.* **2020**, *6*, eabb2891.
(46) Jang, H. − J.; Lee, T.; Song, J.; Russell, J.; Li, H.; Dailey, J.; Searson, P. C.; Katz, H. E. Electronic Cortisol Detection Using an Antibody-Embedded Polymer Coupled to a Field-Effect Transistor. *ACS. Appl. Mater. interfaces* **2018**, *10*, 16233−16237.
(47) Kang, M. − S.; Kang, S. − Y.; Lee, W. − Y.; Park, N. − W.; Kown, K. C.; Choi, S.; Kim, G. − S.; Nam, J.; Kim, K. S.; Saitoh, E.; Jang, H. W.; Lee, S. − K. Large-Scale MoS_2 Thin Films with a Chemically Formed Holey Structure for Ehnahced Seebeck Thermopower and Their Anisotropic Properties. *J. Mater. Chem. A* **2020**, *8*, 8669−8677.
(48) Park, H.; Lee, J.; Han, G.; AlMutairi, A.; Kim, Y. − H.; Lee, J.; Kim, Y. − M.; Kim, Y. J.; Yoon, Y.; Kim, S. Nano-Patterning on Multilayer MoS_2 *via* Block Copolymer Lithography for Highly Sensitive and Responsive Phototransistors. *Commun. Mater.* **2021**, *2*, 1−9.
(49) Zheng, G.; Patolsky, F.; Cui, Y.; Wang, W. U.; Lieber, C. M. Multiplexed Electrical Detection of Cancer Markers with Nanowire Sensor Arrays. *Nat. biotechnol.* **2005**, *23*, 1294−1301.
(50) Kim, A.; Ah, C. S.; Yu, H. Y.; Yang, J.-H.; Baek, I.-B.; Ahn, C.-G.; Park, C. W.; Jun, M. S.; Lee, S. Ultrasensitive, Label-Free, and Real-Time Immunodetection Using Silicon Field-Effect Transistors. *Appl. Phys. Lett.* **2007**, *91*, 103901.
(51) Majd, S. M.; Salimi, A.; Ghasemi, F. An Ultrasensitive Detection of miRNA-155 in Breast Cancer *via* Direct Hybridization Assay Using Two-Dimensional Molybdenum Disulfide Field-Effect Transistor Biosensor. *Biosens. Bioelectron.* **2018**, *105*, 6−13.
(52) Estrada-Y-Martin, R. M.; Orlander, P. R. Salivary Cortisol Can Replace Free Serum Cortisol Measurements in Patients with Septic Shock. *Chest* **2011**, *140*, 1216−1222.
(53) Jiang, C.; Wang, G.; Hein, R.; Liu, N.; Luo, X.; Davis, J. J. Antifouling Strategies for Selective *in Vitro* and *in Vivo* Sensing. *Chem. Rev.* **2020**, *120*, 3852−3889.
(54) Wang, G.; Han, R.; Li, Q.; Han, Y.; Luo, X. Electrochemical Biosensors Capable of Detecting Biomarkers in Human Serum with

https://doi.org/10.1021/acsnano.1c08255
ACS Nano 2022, 16, 1826−1835

Unique Long-Term Antifouling Abilities Based on Designed Multifunctional Peptides. *Anal. Chem.* **2020**, *92*, 7186−7193.

Recommended by ACS

Building a Versatile Platform for the Detection of Protein–Protein Interactions Based on Organic Field-Effect Transistors

Nastaran Yousefi, Simon Rondeau-Gagné, *et al.*

SEPTEMBER 21, 2022
ACS APPLIED ELECTRONIC MATERIALS

READ

Passivation Strategies for Enhancing Solution-Gated Carbon Nanotube Field-Effect Transistor Biosensing Performance and Stability in Ionic Solutions

Faris M. Albarghouthi, Aaron D. Franklin, *et al.*

OCTOBER 04, 2022
ACS APPLIED NANO MATERIALS

READ

Competitive Impedance Spectroscopy in a Schottky-Contacted ZnO Nanorod Structure for Ultrasensitive and Specific Biosensing in a Physiological Analyte

Bhaswati Chakraborty, Chirasree RoyChaudhuri, *et al.*

MAY 27, 2022
ACS SENSORS

READ

Biorecognition Layer Based On Biotin-Containing [1]Benzothieno[3,2-*b*][1]benzothiophene Derivative for Biosensing by Electrolyte-Gated Organic Field-Effect Tra...

Elena Yu. Poimanova, Sergey A. Ponomarenko, *et al.*

MARCH 31, 2022
ACS APPLIED MATERIALS & INTERFACES

READ

Get More Suggestions >

https://doi.org/10.1021/acsnano.1c08255
ACS Nano 2022, 16, 1826−1835